Dynamic Resource Allocation in UAV-enabled mmWave Communication Networks

Sidharth Kumar, Suraj Suman, and Swades De

***Abstract*—Unmanned aerial vehicle (UAV)-enabled cellular architecture over millimeter wave (mmWave) frequency band is likely to be the best solution for on-demand high data rate service provisioning in the next generation communication networks. The beam formed by mmWave antenna array is highly directional and requires multiple beam scans to cover the entire area. This work presents a novel sectoring approach to ensure coverage of the whole area. The side lobe gain of antenna array is taken into consideration, which generates substantial interference in other sectors. The expression for probability distribution of signal-to-interference-plus-noise ratio due to simultaneous transmissions in different sectors is derived in downlink communication scenario. To limit interference in concurrent transmission strategy, a threshold on power spillage from adjacent sectors is placed. For this topology, resource allocation problem is formulated aiming to maximize the sum rate while ensuring minimum rate guarantee to each user. It is observed that sum rate variation with height is unimodal. The sum power and backhaul capacity constraints are accounted. This optimization problem is a mixed-integer non-convex programming. Hence, it is solved using Lagrangian dual decomposition method, which provides asymptotic global optimal solution. Since this method is computationally intensive, a sub-optimal solution is proposed. Simulation results demonstrate convergence to an optimal solution, and it is observed that backhaul link capacity restricts the sum rate. Numerical results are presented for multiple representative field environments consisting of different types of built-up areas. It is observed that the transmitter antenna array sidelobe has a strong impact on the performance as compared to the ideal scenario without sidelobe, which overestimates the total sum rate by a factor of 3.**

***Index Terms*—mmWave, unmanned aerial vehicle, subcarrier assignment, resource allocation, non-convex optimization.**

I. Introduction

In the next generation communication network, to support various internet of things (IoT) devices used in different applications, such as, health monitoring, industry automation, disaster rescue, personal entertainment, and autonomous driving, several orders of magnitude increase in data rate is expected [1]–[3]. These applications have very stringent quality-of-service (QoS) requirements, such as very high throughput, very low latency, and very high reliability. Huge bandwidth is required to satisfy these constraints, which is not impossible with the existing microwave based cellular framework due to the spectrum crisis [4]. To this end, the millimeter wave (mmWave) frequency spectrum that lies between the microwaves and the infrared waves is being explored to support the data-intensive applications in 5G-and-beyond networks. Significantly large bandwidth, low interference, small component size, low cost, are some outstanding features of mmWave, that make it suitable for bandwidth-intensive applications. Moreover, a large number of antenna elements can be packed in a small physical dimension, which also helps in miniaturization of devices. The efforts on standardization of mmWave are making progress, with already available standards like IEEE 802.11ad [5] and wireless HD [6].

Notwithstanding the above-mentioned advantages, blockage from the physical objects, such as trees and buildings, is a major drawback of mmWave. Besides, severe attenuation due to smaller wavelength and high absorption as well as penetration loss from obstacles limits the transmission range [7]. However, the penetration loss can be overcome in mmWave by deploying multiple antenna elements at both transmitter and receiver ends, which offer a high directive gain. Thus, the advantages and tunable features of mmWave make it a suitable technology to satisfy the stringent QoS requirements in the upcoming data-intensive applications.

A. Related works

Recently, mmWave communication network has received a lot of attention from both industry and academia. Previous works mainly focused on channel measurement [8], [9], system performance analysis [10], [11], interference management [12], [13], wireless backhaul [14], [15], and resource allocation [16], [17]. Statistical channel models for mmWave bands were reported in [8] using extensive experimental measurements in indoor and outdoor environment scenarios. Remarkable increase in capacity over current state-of-the-art 4G networks was demonstrated in [9]. Coverage and rate support were analyzed in [10] by considering the deployment of base stations (BSs) as point process, with both line-of-sight (LOS) and non-line-of-sight (NLOS) BSs modeled as independent processes. Spatial frequency reuse and interference level were evaluated in mmWave indoor wireless network [11], whereas dynamic beam switching and static beam selection schemes were presented in [12] to overcome the effect of interference caused by multiuser simultaneous transmission. In these works, it was observed that interference from simultaneous transmission to multiple users can be limited significantly by effectively coordinating the transmitting beams.

The use of mmWave spectrum has also been explored for high-capacity wireless backhaul link to small-cell BSs [14] and relays [15]. A beam alignment method using hierarchical codebooks were presented in [14] to increase coverage of a narrow beam. The authors in [15] designed a wireless relayed backhaul in the mmWave frequency band to enhance coverage range. Joint power and channel allocation was studied in

The authors are with the Department of Electrical Engineering, Indian Institute of Technology Delhi, New Delhi, India.

[16] for smart home mmWave network to deliver multimedia content, with an objective to maximize the network utility. The study in [17] proposed to maximize the minimum throughput of each user in an indoor mmWave networking scenario. The use of microwave and mmWave band dual-mode BS was studied in [13], where significant improvement in number of served users was observed.

Although high directivity improves the performance of users having line-of-sight (LOS) connectivity with the transmitter, the performance of users located in non line-of-sight (NLOS) regions is of concern. This issue becomes severe with the static deployed BSs, because the users with NLOS connectivity will continue to suffer. To overcome this issue, mobile BS mounted on an unmanned aerial vehicle (UAV) is a potent alternative. The choice of UAV lies in its several properties, such as excellent maneuverability, remote controllability, low cost, lightweight, and programming flexibility [18], [19]. These features allow the UAV-mounted BS to change its location as well as altitude to ensure better connectivity to the users [20], [21]. In addition, they do not require any pre-installed infrastructure; they can be deployed within a short time span. Thus, UAV-mounted BS is a cost-effective and reconfigurable architecture to facilitate wireless connectivity. This is an effective solution especially in hard-to-reach deployment scenarios having no electricity and cellular infrastructure. Further, UAV-mounted BS plays a pivotal role in ensuring performance guarantee in the areas with temporarily insufficient capacity of the conventional communication infrastructure, such as during social or sports gathering; mitigating traffic overloading, and disaster relief scenarios.

Recently, the use of UAVs as aerial BSs in 4G LTE for providing wireless coverage have gained considerable attention [22]–[26]. A 3-D cellular architecture, for UAV-enabled BS along with network planning, full coverage, and frequency reuse factors were derived [22]. Optimal deployment algorithm was proposed to maximize the quantity of covered users with a minimum power budget [23]. In [24], performance analysis of a UAV-mounted BS coexisting with device-to-device network was carried out by evaluating sum rate and coverage probability. An algorithm was proposed to estimate the optimal deployment height satisfying coverage, backhaul, and traffic load constraint [25]. Different UAV control mechanisms along with protocol architecture for hierarchical UAV networks are presented in [26] To this end, we believe that, the UAV-mounted BS operating at mmWave frequency bands will be a promising architecture to satisfy the stringent QoS requirements in upcoming wireless networks.

The concept of mUBS was employed in [27]–[36] to fulfill stringent user QoS requirements. In [27], optimal resource allocation problem for uplink non-orthogonal access to UAV-enabled BS is solved by considering subchannel assignment, transmit power, and UAV flying height. The work in [28] maximizes the achievable sum rate of all users, subject to a minimum rate constraint for each. A non-orthogonal multiple access scheme was proposed in [29] to simultaneously serve multiple users during a temporary sports event. An algorithm to find optimal coverage radius and efficiently allocate radio resources in UAV-aided heterogeneous cellular network was presented in [30]. The study in [31] proposed to deploy UAV as an aerial relay node to enable dynamic routing in mmWave backhaul links, thereby mitigating blockage due to random mobility of blocking users. In [32], the locations of transceivers in downlink and uplink were modeled respectively using Poisson point processes and Poisson cluster processes to derive closed-form expressions of the coverage probability in the uplink and the downlink. A tractable three-dimensional (3D) spatial model was proposed in [33] for evaluating the average downlink performance of UAV networks at mmWave bands. In [34], outage probability was evaluated at mmWave and at sub-6 GHz frequency in different blockage environments and UAV heights, to address the capacity demand of the fronthaul network. In [35], joint downlink simultaneous wireless information and power transfer and uplink information transfer in UAV-assisted mmWave cellular networks was presented. The authors in [36] studied secure mmWave communication assisted by multiple UAV-enabled relays and jammers, where multiple eavesdroppers on ground are randomly distributed. For a quick summary, a brief highlight of the main features considered in these reported works related to mUBS vis-a-vis our current study is presented in Table I.

B. Motivation and contributions

We consider deployment of mUBS over mmWave bands for communication service to a large gathering of user population, such as in sports events or social congregations, where there is a short and sudden increase in data traffic demand. A large number of antenna elements can be placed on mUBS due to smaller wavelength of mmWave bands, which offers directive and steerable beams with very high gain. Although the main lobe provides very high directivity, the negative effect of side lobes cannot be neglected as they cause interference in adjoining areas. The works reported in [29]–[31] assumed an idealized model of antenna array gain and neglected the effect of side lobes, which is not the case in real-life deployments. Ignoring the effect of side lobes may lead to under-resource provisioning, and hence this parameter should be taken into account while analyzing the system performance. Further, the works reported in [28]–[30], [32]–[36] do not consider capacity limitation of the backhaul link, although the mUBS is provisioned as an aerial relay node working to provide a flexible and reconfigurable backhaul connectivity.

This paper deals with dynamic resource allocation for mUBS by considering the practical constraints, thereby aiming to design a more realistic system. In view of data-intensive services, the analysis in the paper also provides an estimate on the backhaul link capacity that is required to be made available while planning mmWave-based cellular network.

The major contributions of this work are as follows:

- A sectoring method to cover a given region is presented and a closed-form expression for the required number of antenna array elements is evaluated. Probability distribution of signal-to-interference-plus-noise ratio (SINR) is obtained by accounting for the antenna side lobe gain.
- Concurrent transmission in each sector through multiple antenna sub-arrays will generate interference to the users

Table I: A brief summary of main features considered in different reported works as compared to the proposed approach.

Feature	Prior Art	Current Work
Interference due to antenna side lobes	Considered in [32], [34], [35], [36] Not considered in [27], [28], [29], [30], [31], [33]	Considered
Capacity of backhaul link	Considered in [31] Not considered in [27], [28], [29], [30], [32], [33], [34], [35], [36]	Considered
Rate guarantee to each user	Considered in [28], [29], [30] Not considered in [27], [31], [32], [33], [34], [35], [36]	Considered

in other sectors through the side lobes, whereas transmission in purely time division approach will incur high latency and is inefficient in spectrum usage. To achieve a trade-off we use interference-limited transmission strategy, where the interference caused through side lobes is restricted within a threshold.

- An optimization problem is formulated to maximize the sum rate achieved by all the users considering a minimum rate guarantee and backhaul link constraint. To solve this mixed-integer non-convex programming, Lagrangian dual decomposition method is presented which offers asymptotically global optimal solution due to zero duality gap for large number of subcarriers. Also, a sub-optimal solution motivated by water-filling analogy is presented, which is computationally efficient.
- The simulation results are presented to assess the performance of mUBS. It is observed that, interference-limited simultaneous transmission based mUBS can serve a large number of users with a minimum rate requirement and limited power budget. The asymptotically-optimal and proposed low-complexity sub-optimal solutions are shown to perform significantly well with respect to the two benchmark schemes, namely, random subcarrier allocation and equal power allocation.

C. Scope

It is notable that, the primary focus in this study is to evaluate the maximum achievable downlink sum rate in a terrestrial cell area served by a mUBS under practical antenna radiation patterns. While the sum rate performance is expected to be poorer in presence of UAV hovering and other environmental uncertainties, accounting for these factors is out of scope of the current work.

D. Organization

The rest of the paper is organized as follows. Section II presents the antenna array model and sectoring method along with the analytical derivation of probability distribution of SINR. The optimization problem formulation and the different solution techniques are presented respectively in Sections III and IV. Numerical results for the proposed solution methods are discussed in Section V. Finally, concluding remarks are drawn in Section VI. Table II lists all the major notations used in the paper along with their descriptions.

II. System Model

Fig. 1 shows a typical deployment scenario of mUBS over mmWaves, where mUBS is deployed to serve a sudden surge of traffic demand from a temporary gathering of user population. The antenna array mounted on mUBS serves the users located in a circle of radius $\mathcal{R}_a$ through directional beams. The UAV is considered hovering at altitude h and wirelessly connected to a terrestrial BS for backhaul connectivity.

The usage of UAV has several benefits in high data rate demand scenarios. UAV offers LOS connectivity to the users in the fronthaul link and it can adjust its altitude according to the user data demand in order to satisfy the QoS. Apart from this, it requires a backhaul link with sufficient capacity

Table II: List of major notations with their description.

$\mathcal{R}_a$	Radius of circular coverage area
h	Hovering altitude of mUBS
N	Number of antenna array elements
ϕ	Azimuth direction angle for antenna array
θ	Elevation direction angle for antenna array
θ_i	Offset angle
θ_h	Half beam width in azimuth direction
d	Absolute distance between mUBS and ground user
G_{tx}	Gain of the transmitter antenna
G_{rx}	Gain of the receiver antenna
P_{tx}	Transmit power of mUBS
H_k^n	Square of downlink channel gain to user k over subcarrier n
P_k^n	Power transmitted over subcarrier n while serving user k
$r_{n,k}$	Data rate for user k over subcarrier n
$\pi_{n,k}$	User-subcarrier association variable
R_o	Minimum rate guarantee to each user to maintain fairness
R_{max}^{bh}	Capacity restriction of backhaul link of mUBS
I_{th}	Interference limit in downlink transmission for each sector
$\alpha, \beta, \gamma, \zeta$	Lagrange multipliers
$\delta^{(i)}$	Step size at i^{th} iteration

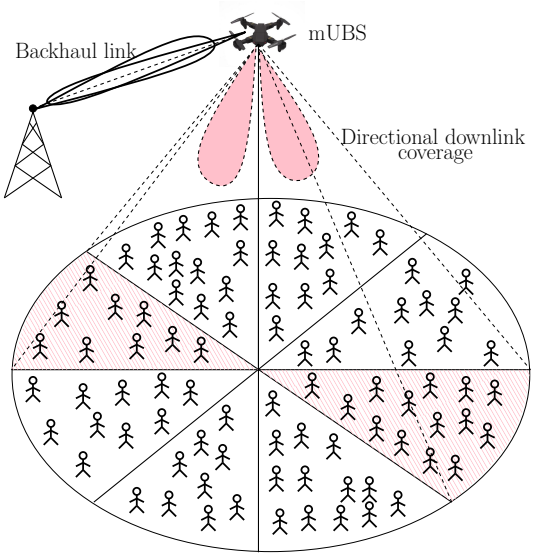

Figure 1: System model for wireless coverage provisioning through mUBS in congested area.

to fulfill the demands of users. Excellent maneuvering capability of UAV enables it to establish a LOS connectivity with the neighboring traditional cellular BS to enhance the capacity of backhaul link. Further, UAV-enabled BS offers a re-configurable architecture for providing on-demand service within a short time span. Multiple UAVs or a swarm of UAVs can also be deployed quickly if a single UAV is not able to satisfy the QoS. These features cannot be realized by a terrestrial BS which is statically deployed at a fixed altitude and hence cannot always ensure LOS connectivity to the users due to surrounding infrastructure and obstacles.

A. Antenna array model

An antenna array comprises of a set of small radiating elements to ensure a specific radiation pattern. The total electric field generated by the array is a vector sum of the field by individual elements. The fields add constructively in the main lobe and hence have high gain, whereas the side lobe fields add non-coherently and hence have less gain. Thus, a uniform antenna array having equally spaced antenna elements with equal feed current can be modeled to act as a single directional antenna. In this work, planar antenna array is used to facilitate mmWave communication.

1) Uniform square array: A square planar antenna array can be formed by placing multiple linear arrays beside each other. The antenna arrays have a uniform spacing of half-wavelength, which avoids the unnecessary grating lobes other than the main lobe. It is notable that a square antenna geometry is chosen among the other possibilities (e.g. linear array, circular, etc.), because from standard antenna theory it has been proven that, to pack a particular number of antenna elements with half wavelength spacing, square array requires the least area and hence the least size requirement on UAV. For an array with asymptotically large number of antenna elements, the gain in the main beam is equal to N, where N is the number of antenna elements. Further, the half power beamwidth in both azimuth (ϕ) and elevation (θ) plane is equal to $\frac{\pi}{\sqrt{N}}$[37]. The antenna gain $F(\theta,\phi)$ is a function of elevation angle ($\theta \in [-\pi/2, \pi/2]$) and azimuth angle ($\phi \in [-\pi, \pi]$). As the total energy is conserved in electromagnetic transmission, the antenna gain function must satisfy: $\int_{-\pi}^{\pi}\int_{-\pi/2}^{\pi/2} F(\theta,\phi)\cos(\theta)d\theta d\phi = 4\pi$. Then, the gain in main and side lobe is evaluated as follows:

$$F(\theta,\phi) = \begin{cases} N, & \text{if } \theta \in [-\sqrt{\frac{\pi}{N}}, +\sqrt{\frac{\pi}{N}}] \\ & \text{and } \phi \in [-\sqrt{\frac{\pi}{N}}, +\sqrt{\frac{\pi}{N}}], \\ \frac{1-\frac{\sqrt{N}}{2}\sin\frac{\pi}{2\sqrt{N}}}{1-\sin\frac{\pi}{2\sqrt{N}}}, & \text{otherwise.} \end{cases} \quad (1)$$

A pictorial depiction of derived antenna gain pattern in (1) is shown in Fig. 2(a).

2) Lateral projection of antenna beam on ground: Based on the radiation pattern of antenna, it is important to evaluate the area covered by antenna radiation on ground plane. The area covered by a lateral projection from mUBS could be of two types, as shown in Fig. 2(b) and Fig. 2(c).

For the first case (see Fig. 2(b)), some area in a patch remains uncovered. The critical parameters, i.e., inner and outer

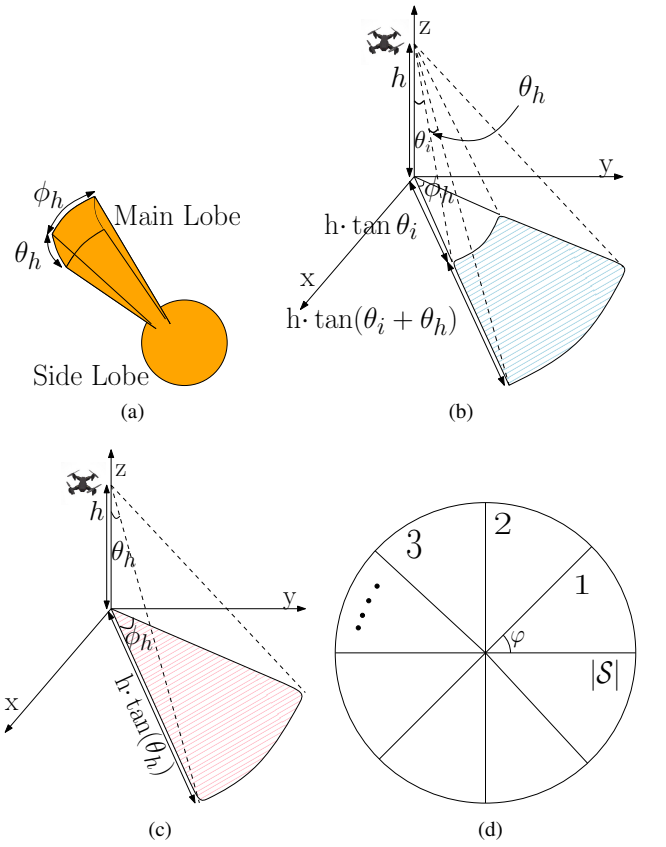

Figure 2: (a) The beam formed by directional antenna array; two possible lateral projections of antenna beam on ground in (b) and (c); (d) partitioning of a given circular area into different sectors.

radius, are respectively $h\tan(\theta_i)$ and $h\tan(\theta_i+\theta_h)$, where θ_i is the offset angle and θ_h would be the half beamwidth of antenna array in azimuth direction. This coverage scenario is a more general case of user region considered in [29], where the authors considered a uniform linear array instead of square array. For the second case (see Fig. 2(c)), the offset angle is zero, hence the coverage radius is given as $r = h\tan(\theta_h)$. Based on partitioning approach shown in Fig. 2(c), the whole area can be divided into $|\mathcal{S}|$ number of sectors as shown in Fig. 2(d).

The number of beam steers need to be calculated to cover the whole circular area. For this purpose, a spherical structure having center at UAV can be assumed, and the solid angle made by a circular patch of radius r on ground at the UAV is obtained as:

$$\Omega_r = \frac{1}{2}\Big(1 - \frac{r}{\sqrt{r^2+h^2}}\Big). \quad (2)$$

Thus, the minimum number of beam steers N_{beams} is found as:

$$N_{beams} = \left\lceil \frac{\Omega_r}{\Omega_A} \right\rceil = \left\lceil \frac{N}{2\pi}\Big(1 - \frac{r}{\sqrt{r^2+h^2}}\Big) \right\rceil \quad (3)$$

where Ω_A is the solid angle made by the antenna main lobe. This is the product of half power beamwidth in both elevation and azimuth directions, i.e., $\Omega_A = \phi_h \times \theta_h$, where $\lceil\cdot\rceil$ denotes the ceiling function.

B. Air-to-ground mmWave channel model

The channel model between mUBS and ground user is quite different from the terrestrial channel model used in conventional cellular networks due to mobility of UAV. In the literature, there are only a few works that considered the air-to-ground (AtG) path loss model at mmWave frequencies [38]–[40]. It was observed that the characteristics of AtG and terrestrial channel models are similar for the government allowed UAV heights. The path loss of LOS (PL_{LOS}) and NLOS (PL_{NLOS}) components in dB at mmWave frequencies follow a statistical model given as [9]:

$$\begin{aligned} PL_{LOS}(h,\theta) &= 61.4 + 10 \cdot 2 \log_{10}(d) + \mathcal{N}(0, 33.64) \quad (4) \\ PL_{NLOS}(h,\theta) &= 72.0 + 10 \cdot 2.92 \log_{10}(d) + \mathcal{N}(0, 75.69) \end{aligned}$$

where $\mathcal{N}(\mu, \sigma^2)$ denotes the normal random distribution with mean μ and variance σ^2. $d = \sqrt{h^2 + r^2}$ is the absolute distance between mUBS and a ground receiver (user). Antenna beam gains are not considered in this path loss model. The NLOS component have higher path loss exponent as well as more shadowing loss as it has to travel more distance and go through more obstructions, such as from trees and buildings, before reaching to the ground user, resulting in more reflection and diffraction to the signal. Based on the above formulation, the received power at any ground user is:

$$P_{rx} = P_{tx} - PL(h,\theta) + G_{tx} + G_{rx} \text{ [in dB]} \quad (5)$$

where G_{tx} and G_{rx} are antenna gains of transmitter and receiver antennas, respectively, and are computed from (1). P_{tx} is the transmitted power. The path loss $PL(h,\theta)$ corresponding to the LOS and NLOS components is selected based on availability or lack of line of sight.

C. Downlink SINR distribution

Using the radiation pattern of antenna array and the path loss model discussed in previous subsections, the SINR in downlink scenario at a user due to simultaneous transmission is evaluated. The downlink SINR according to the proposed sectoring approach (cf. Fig. 2(d)) is expressed as:

$$SINR = \frac{P_{rx-ml}}{N_o + \sum_{i=1}^{|\mathcal{S}|} P_{rx-sl}} = \frac{\mathbb{X}}{\mathbb{Y}} \quad (6)$$

where P_{rx-ml} is the power received from transmission along the main lobe. P_{rx-sl} is the power received from transmission in side lobe of other sectors, which is responsible for interference. The only difference between the signal in main lobe and side lobe is due to different respective antenna gain. N_o is the noise power. To evaluate the distribution of SINR, first the distributions of $\mathbb{X}$ and $\mathbb{Y}$ are evaluated. Note that, the main objective in this work is to evaluate the interference caused by the side lobes due to concurrent air-to-ground transmission in multiple sector over mmWave bands. The deployment scenario is considered in areas where conventional communication infrastructure is unavailable or temporarily insufficient, where the other sources of mmWave interference are expected to be very less. Hence, such interference is not accounted in the SINR computation.

The path loss for LOS and NLOS components consist of a distance dependent term and a zero mean Gaussian normal random variable (cf. (4)).. Therefore, the pathloss (in dB scale) is also a normal random variable, though with a non-zero mean. The received power (in dB scale) is a linear function of path loss (cf. (6)) and hence it is also a normal random variable. Hence, depending on the availability or lack of LOS component, the mean μ and variance σ of received power over the main lobe and side lobes are obtained as follows:

$$\begin{aligned} \mu_{P_{rx-ml}} &= \begin{cases} \ln(P_{tx}G_{main}G_{rx}) - \frac{\ln(10)}{10}(61.4 + 20\log_{10}(d)), \text{LOS} \\ \ln(P_{tx}G_{main}G_{rx}) - \frac{\ln(10)}{10}(72.0 + 29.2\log_{10}(d)), \text{NLOS} \end{cases} \\ \sigma^2_{P_{rx-ml}} &= \sigma^2_{P_{rx-sl}} = \begin{cases} \left(\frac{\ln 10}{10}\right)^2 \cdot 33.64, \text{ LOS} \\ \left(\frac{\ln 10}{10}\right)^2 \cdot 75.69, \text{ NLOS} \end{cases} \\ \mu_{P_{rx-sl}} &= \begin{cases} \ln(P_{tx}G_{side}G_{rx}) - \frac{\ln(10)}{10}(61.4 + 20\log_{10}(d)), \text{LOS} \\ \ln(P_{tx}G_{side}G_{rx}) - \frac{\ln(10)}{10}(72.0 + 29.2\log_{10}(d)), \text{NLOS} \end{cases} \end{aligned} \quad (7)$$

where G_{main} and G_{side} are the gain of main and side lobe as obtained by (1). The factor $\ln(10)$ appears due to conversion from base 10 to natural logarithm. Hence, the numerator $\mathbb{X}$, which is the power received through main lobe, also follows lognormal distribution with mean $\mu_{\mathbb{X}} = \mu_{P_{rx-ml}}$ and variance $\sigma_{\mathbb{X}} = \sigma^2_{P_{rx-ml}}$.

The denominator of SINR, $\mathbb{Y}$ is a sum of random variables and a noise power term. The noise power is constant for a given bandwidth, and hence it can be considered as a random variable with zero variance. On linear scale, it follows lognormal distribution having mean $\ln(N_o)$ and zero variance. Thus, the denominator of SINR, $\mathbb{Y}$ can be considered as a sum of random variables where each has lognormal distribution with different mean and variance. In the literature, the distribution of sum of lognormal random variables is not known, but approximations with good fitting are available, which also follow the lognormal distribution [41]. The approximation works very well except for the cases with the distributions having very high variance. The mean μ_d and variance σ_d^2 of sum of τ lognormal random variable are given as:

$$\sigma_d^2 = \ln\left[\frac{\sum_{i=1}^{\tau}\exp(2\mu_i + \sigma_i^2)(\exp(\sigma_i^2) - 1)}{[\sum_{i=1}^{\tau}\exp(\mu_i + \sigma_i^2/2)]^2} + 1\right] \quad (8)$$

$$\mu_d = \ln\left[\sum_{i=1}^{\tau}\exp(\mu_i + \sigma_i^2/2)\right] - \frac{\sigma_d^2}{2} \quad (9)$$

where μ_i and σ_i^2 are the mean and variance of individual lognormal distributions (cf. (7)), which are being added. Here, $\tau = |\mathcal{S}| + 1$. Hence, the denominator $\mathbb{Y}$ is also lognormally distributed with mean $\mu_{\mathbb{Y}} = \mu_d$ and variance $\sigma^2_{\mathbb{Y}} = \sigma_d^2$.

Thus, both $\mathbb{X}$ and $\mathbb{Y}$ follow the lognormal distribution. Therefore, SINR will also follow the lognormal distribution as the ratio of two lognormal distributions is also a lognormal distribution, with $\mu_{SINR} = \mu_{\mathbb{X}} - \mu_{\mathbb{Y}}$, $\sigma^2_{SINR} = \sigma^2_{\mathbb{X}} + \sigma^2_{\mathbb{Y}}$. Hence, the distribution of SINR in linear scale is given as:

$$f_{SINR}(z) = \frac{1}{z\sqrt{2\pi\sigma^2_{SINR}}} \exp\left[\frac{-(\ln z - \mu_{SINR})^2}{2\sigma^2_{SINR}}\right]. \quad (10)$$

Using the distribution of SINR, the outage probability for a particular user is given as:

$$P_{out}(h,\theta) = \mathbb{P}(SINR \leq \beta) = \frac{1}{2}\left[1 + \text{erf}\left(\frac{\ln(\beta - \mu_Z)}{\sqrt{2\sigma_Z^2}}\right)\right], \tag{11}$$

where $\text{erf}(\cdot)$ is the standard error function defined as $\text{erf}(z) = \frac{2}{\sqrt{\pi}}\int_z^0 e^{-t^2}dt$. Comparison of analytically-obtained SINR distribution and that via simulations is discussed in Section V-A.

D. Network coverage topology

The purpose of deploying mUBS is to provide better quality of service in a congested area. As mentioned in the system model (see Fig. 1), the target coverage area is considered to be circular of radius $\mathcal{R}_a$. This circular region is divided into sectors (see Fig. 2(d)) for smoother coverage. The whole area can be covered either by having multiple sub-arrays for each sector or by steering a single beam towards each sector. The main lobe of antenna array can be easily steered in desirable direction by just introducing sequential time delay or phase variations to signal being fed into the antenna array elements [42]. The average latency T_d is approximately: $T_d \approx T_s \times |\mathcal{S}|$, where T_s is the service time allocated to a single sector. But, this strategy is not suitable for real-time applications, such as video streaming, augmented reality, etc., because the users will face unacceptable large latency in service as the beam needs to be swept over all the sectors. This can be thought of as total time of antenna array is being divided among different sectors, hence it is named as time division strategy.

On the other hand, the strategy with independent sub-array for each sector requires proper attention to mitigate the interference (both inter-sector and intra-sector). To mitigate intra-sector interference, orthogonal multi-access techniques are employed, whereas limitation on power transmission or intelligent frequency assignment is done to mitigate the interference from other sectors. As the transmission is happening over all the different sectors using independent antenna arrays, it is termed as concurrent transmission strategy. *"How many elements should each sub array have?"* is an important question for this kind of deployment. Referring to Fig. 2(d), φ is related to the number of antennas by two factors: one is half-power beamwidth $\varphi = \frac{\pi}{\sqrt{\mathfrak{N}}}$, and the other is coverage guarantee of whole region $\mathcal{R}_a = h\tan(\varphi)$. Hence, the exact number of antenna elements $\mathfrak{N}$ in each sub-array is evaluated as:

$$\mathfrak{N} = \left(\frac{\pi}{\tan^{-1}(\frac{\mathcal{R}_a}{h})}\right)^2. \tag{12}$$

Then, the total number of antenna elements required to cover the whole region simultaneously, is: $N = \mathfrak{N} \times |\mathcal{S}|$.

It is important to decide between the choice of concurrent transmission and time division transmission. The interference is the main bottleneck in concurrent transmission, whereas waiting time or latency is the main bottleneck in time-division based transmission. In concurrent transmission all sectors of the entire region are simultaneously covered by different set of antenna elements. Due to full frequency reuse in all sectors, the signal quality in a sector is affected by the side lobe interference from the other sectors, which is in addition to the additive noise. For time-division transmission, since only one sector is covered at a time and all orthogonal frequency division is employed within a sector, there is no interference experienced.

Since in this work we focus on the mmWave frequencies, high propagation loss of mmWave signal has to be accounted as compared to the transmission in traditional sub-6 GHz frequencies. However due to the smaller wavelength more number of antennas can be packed into a small area resulting in high antenna array gains for the main lobe and lower gains for the side lobs. Hence, in this work, we deploy concurrent transmission strategy and further limit the interference below a threshold. To limit spilling of unnecessary power to adjoining sectors it requires that,

$$P_{rx}(h,\theta,R_a,P_{tx}) \leq I_{th} \Rightarrow P_{tx,min} = P_{rx}^{-1}(I_{th},h,\theta,R_a) \tag{13}$$

where $P_{rx}(h,\theta,R,P_{tx})$ is the power received at a user making an angle θ with mUBS and I_{th} is the interference threshold.

III. Resource Allocation Problem Formulation

For the concurrent transmission strategy introduced in last section, resource allocation over a scheduling time T_S needs to be done for the users located in the coverage area. The main objective is to maximize the total sum rate of all users with a maximum power budget. Besides, to maintain fairness among the users, a certain minimum rate guarantee is ensured. Also, the backhaul capacity is taken into consideration, because UAV-mounted transmitter does not have a high-speed optical fiber link.

Let H_k^n be the square of channel gain from UAV to user k over subcarrier (SC) n, without considering the antenna gain. H_k^n includes the effect of path loss, shadowing, and fading parameters. Here, Nakagami fading is considered due to strong LOS component in mmWave wireless networks. P_k^n is the power transmitted over n^{th} SC while serving the k^{th} user. Thus, the data rate $r_{n,k}$ for user k over SC n is expressed as:

$$r_{n,k} = \log_2\left(1 + \frac{P_k^n G_{main} H_k^n}{N_o + \sum_{i\neq k}^{|\mathcal{S}|} P_i^n G_{side} H_i^n}\right). \tag{14}$$

Let $\mathcal{K} = \{1,2,\cdots,K\}$ denote the set of users and $\mathcal{N} = \{1,2,\cdots,\mathbb{N}\}$ denote the set of orthogonal subcarriers that are distributed among the users of a particular sector. The user-subcarrier association variable $\pi_{n,k}$ is defined as:

$$\pi_{n,k} = \begin{cases} 1, & \text{if user } k \text{ is assigned to SC } n, \\ 0, & \text{otherwise.} \end{cases} \tag{15}$$

Consequently, the optimization problem for maximizing the sum rate over all users located in the coverage area is stated as:

$$(\mathcal{P}_1): \underset{\pi_{n,k},P_k^n}{\text{maximize}} \sum_{i=1}^{|\mathcal{S}|}\sum_{k=1}^{K}\sum_{n=1}^{\mathbb{N}} \pi_{n,k} r_{n,k},$$

subject to:

$$(\mathcal{C}1) \quad \sum_{n=1}^{\mathbb{N}}\sum_{k=1}^{k} P_k^n \le P_S,$$

$$(\mathcal{C}2) \quad \sum_{n=1}^{\mathbb{N}} \pi_{n,k} r_{n,k} \ge R_o, \ \forall k \in \mathcal{K},$$

$$(\mathcal{C}3) \quad \sum_{k=1}^{K}\sum_{n=1}^{\mathbb{N}} \pi_{n,k} r_{n,k} \le R_{max}^{bh},$$

$$(\mathcal{C}4) \quad P_k^n \ge 0, \ \forall n \in \mathcal{N}, \ \forall k \in \mathcal{K},$$

$$(\mathcal{C}5) \quad \sum_{k=1}^{K} \pi_{n,k} \le 1, \ \forall n \in \mathcal{N},$$

$$(\mathcal{C}6) \quad \pi_{n,k} \in \{0,1\}, \ \forall n \in \mathcal{N}, \ \forall k \in \mathcal{K},$$

Constraint $(\mathcal{C}1)$ ensures the limit on total transmitted power at mUBS. Constraint $(\mathcal{C}2)$ guarantees minimum rate R_o to each user to maintain fairness, whereas constraint $(\mathcal{C}3)$ accounts for the capacity restriction R_{max}^{bh} of backhaul link of mUBS. Constraint $(\mathcal{C}4)$ ensures the non-negative nature of transmitted power. Constraint $(\mathcal{C}5)$ indicates that a particular subcarrier is assigned to only one user, where the user subcarrier association variables only take binary values, i.e., either 0 or 1.

This optimization is a mixed-integer non-convex programming problem, which is NP-hard [43]. Solving this problem by brute force search over all the solution space is not a feasible option, as well as it is computationally inefficient. This is because it requires to compute $\binom{\mathbb{N}+K}{K}$ subcarrier matching possibilities. This type of process is restrictive to even slightly large number of subcarriers due to excessive computation overhead. Also, for a particular set of user-subcarrier assignment, the power allocation problem is still non-convex due to the inclusion of interference (cf. (14)). To make power allocation problem solvable, a limit on the interference I_{th} in downlink transmission for each sector is placed (cf. (13)). Therefore, the lower bound of rate to a particular user becomes,

$$\tilde{r}_{n,k} = \log_2\Big(1 + \frac{P_k^n G_{main} H_k^n}{N_o + (\tilde{s}-1)\times I_{th}}\Big) \tag{16}$$

where I_{th} is the interference bound on transmission from a particular sector. Due to this, the problem $(\mathcal{P}1)$ for a particular sector is transformed as follows:

$$(\mathcal{P}_2): \underset{\pi_{n,k},P_k^n}{\text{maximize}} \sum_{k=1}^{K}\sum_{n=1}^{\mathbb{N}} \pi_{n,k} \tilde{r}_{n,k},$$

subject to: $(\mathcal{C}1)$, $(\mathcal{C}4)$, $(\mathcal{C}5)$, $(\mathcal{C}6)$,

$$(\mathcal{C}2) \quad \sum_{n=1}^{\mathbb{N}} \pi_{n,k} \tilde{r}_{n,k} \ge R_o, \ \forall k \in \mathcal{K},$$

$$(\mathcal{C}3) \quad \sum_{k=1}^{K}\sum_{n=1}^{\mathbb{N}} \pi_{n,k} \tilde{r}_{n,k} \le R_{max}^{bh},$$

$$(\mathcal{C}7) \quad \sum_{k=1}^{K} P_k^n \Psi_n \le I_{th}, \ \forall n \in \mathcal{N},$$

where constraint $(\mathcal{C}7)$ is introduced to limit the interference caused from transmission in one sector to other concurrent transmitting sector. Ψ_n is the interference factor by which transmission in one sector can interfere with the transmissions in other sectors through side lobes; $\Psi_n = H_k^n G_{side} \pi_{n,k}$. Approach to the solution of $(\mathcal{P}_2)$ is discussed next.

IV. Proposed Solution Methodology

In this section, we solve the optimization problem $(\mathcal{P}_2)$. A detailed procedure to obtain an asymptotically optimal solution is presented, which is based on Lagrangian duality concepts. The procedure for a sub-optimal solution is also presented, which is computationally efficient as compared to the asymptotically-optimal solution.

A. Asymptotically optimal solution

The formulated optimization problem $(\mathcal{P}_2)$ is non-convex due to the mixed-integer constraints $(\mathcal{C}5)$ and $(\mathcal{C}6)$. However, it satisfies the time-sharing conditions which ensure that duality gap is nearly zero for a large number of subcarriers even though the primal problem is non-convex [44]. This observation allows the dual optimal solution to be applicable for the primal problem. Even though the dual problem is always convex [45], it is non-differentiable due to the mixed-integer constraints, and therefore a standard numerical technique of subgradient method is employed to obtain the dual optimal solution, which is presented later in this section.

The Lagrangian $L(\{\pi_{n,k}, P_k^n\}_{\forall n\in\mathcal{N}}, \alpha, \beta, \gamma, \zeta)$ of the problem $(\mathcal{P}_2)$ is formulated as:

$$\begin{aligned}
&L(\{\pi_{n,k}, P_k^n\}_{\forall n\in\mathcal{N}}, \alpha, \beta, \gamma, \zeta) \\
&\underset{(\alpha,\beta,\gamma,\zeta)\ge 0}{} \\
&\quad = \textstyle\sum_{k=1}^{K}\sum_{n=1}^{\mathbb{N}} \pi_{n,k}\tilde{r}_{n,k} - \alpha\Big(\sum_{k=1}^{K}\sum_{n=1}^{\mathbb{N}} P_k^n - P_S\Big) \\
&\qquad\quad - \textstyle\sum_{k=1}^{K} \beta_k (R_o - \sum_{n=1}^{\mathbb{N}} \pi_{n,k}\tilde{r}_{n,k}) \\
&\qquad\quad - \gamma\Big(\sum_{k=1}^{K}\sum_{n=1}^{\mathbb{N}} \pi_{n,k}\tilde{r}_{n,k} - R_{max}^{bh}\Big) \\
&\qquad\quad - \textstyle\sum_{n=1}^{\mathbb{N}} \zeta_n \Big(\sum_{k=1}^{K} P_k^n \Psi_n - I_{th}\Big) \\
&\quad = \textstyle\sum_{n=1}^{\mathbb{N}} L_n(\pi_{n,k}, P_k^n, \alpha, \beta, \gamma, \zeta) + \alpha P_S \\
&\qquad\quad - \textstyle\sum_{k=1}^{K} \beta_k R_o + \gamma R_{max}^{bh} + \sum_{n=1}^{\mathbb{N}} \zeta_n I_{th}
\end{aligned}$$

where α and γ are the Lagrange multipliers for power constraint $(\mathcal{C}1)$ and backhaul constraint $(\mathcal{C}3)$, respectively. $\beta = [\beta_1, \cdots, \beta_K]$ and $\zeta = [\zeta_1, \cdots, \zeta_N]$ are the Lagrange multipliers associated with $(\mathcal{C}2)$ and $(\mathcal{C}7)$, respectively. The dual variables associated with non-equality constraints are always non-negative real numbers in order to satisfy the complementary slackness condition. The positive power constraint mentioned in $(\mathcal{C}4)$ and the binary variable constraint mention in $(\mathcal{C}5)$ are not considered in Lagrangian formulation to avoid unnecessary complexity. However, they are satisfied individually after solving the dual problem, as their exclusion will not affect the solution of dual problem. Further, $L_n(\pi_{n,k}, P_k^n, \alpha, \beta, \gamma, \zeta)$ is expressed as:

$$\begin{aligned}
&L_n(\pi_{n,k}, P_k^n, \alpha, \beta, \gamma, \zeta) \\
&\quad = \textstyle\sum_{k=1}^{K} \pi_{n,k}\tilde{r}_{n,k}(1 + \beta_k - \gamma) - \alpha P_k^n - \zeta_n \Psi_n P_k^n. \quad (17)
\end{aligned}$$

Accordingly, the Lagrange dual function $g(\alpha,\beta,\gamma,\zeta)$ associated with the primal problem $(\mathcal{P}_2)$ is expressed as:

$$g(\alpha,\beta,\gamma,\zeta) \triangleq \underset{\pi_{n,k},P_k^n}{\text{maximize}}\ L(\{\pi_{n,k},P_k^n\}_{\forall n\in\mathcal{N}},\alpha,\beta,\gamma,\zeta). \tag{18}$$

Hence, the Lagrange dual optimal associated with primal problem $(\mathcal{P}_2)$ is obtained as:

$$L^*_{dual} = \underset{\alpha,\beta,\gamma,\zeta}{\text{minimize}}\ g(\alpha,\beta,\gamma,\zeta). \tag{19}$$

Our aim is to find the optimal value of Lagrange dual, i.e., L^*_{dual}, and for this purpose the problem in (19) is decomposed into two sub-problems and optimized sequentially. The first sub-problem maximizes the Lagrangian $L(\{\pi_{n,k},P_k^n\}_{\forall n\in\mathcal{N}},\alpha,\beta,\gamma,\zeta)$ to obtain the Lagrange dual function $g(\alpha,\beta,\gamma,\zeta)$. However, solving first problem mentioned in (18) is equivalent to maximizing $L_n(\pi_{n,k},P_k^n,\alpha,\beta,\gamma,\zeta)$ independently for each SC, and this can be stated as follows:

$$\begin{aligned}(\mathcal{P}_{\mathbf{3}}):\ &\underset{\pi_{n,k},P_k^n}{\text{maximize}}\ L_n(\pi_{n,k},P_k^n,\alpha,\beta,\gamma,\zeta),\\ &\text{subject to:}\quad (\mathcal{C}4),(\mathcal{C}5),\ \text{and}\ (\mathcal{C}6).\end{aligned} \tag{20}$$

Assuming (n,k) is a valid subcarrier-user pair, i.e., n^{th} subcarrier is allotted to the k^{th} user, $(\mathcal{P}_3)$ is further reduced as follows:

$$\begin{aligned}(\mathcal{P}_{\mathbf{4}}):\ &\underset{P_k^n}{\text{maximize}}\ \pi_{n,k}\log_2\Big(1+\frac{P_k^nG_{main}H_k^n}{N_o+(\tilde{s}-1)\times I_{th}}\Big)\\ &\qquad\times(1+\beta_k-\gamma)-\alpha P_k^n-\zeta_n\Psi_nP_k^n,\\ &\text{subject to:}\quad (\mathcal{C}4).\end{aligned} \tag{21}$$

There would be N such independent sub-problems for each subcarrier. Thus, a total of $N\times K$ independent power allocation problems need to be solved for a particular set of values of dual variables $(\alpha,\beta,\gamma,\zeta)$. The problem defined in (21) is a convex optimization problem, and its exact solution is obtained as follows:

$$P_k^{n*} = \left[\frac{(1+\beta_k-\gamma)\pi_{n,k}}{\ln(2)(\alpha+\zeta_n\Psi_n)} - \frac{N_o+(\tilde{s}-1)\times I_{th}}{H_k^nG_{main}}\right]^+ \tag{22}$$

where $[\cdot]^+$ is the rectifier function, such that $[\chi]^+ = max(0,\chi)$. By only considering the positive values of P_k^{n*}, the positive power constraint mentioned in $(\mathcal{C}4)$ is automatically satisfied.

After finding the optimal power for each subcarrier-user association possibilities, the optimal $\pi_{n,k}$ is found out solving the following problem:

$$\begin{aligned}(\mathcal{P}_{\mathbf{dual}}):\ &\underset{\pi_{n,k}}{\text{maximize}}\ L(\{\pi_{n,k},P_k^{n*}\}_{\forall n\in\mathcal{N}},\alpha,\beta,\gamma,\zeta),\\ &\text{subject to:}\quad (\mathcal{C}5)\ \text{and}\ (\mathcal{C}6).\end{aligned} \tag{23}$$

The optimal user-subcarrier association $\pi^*_{n,k}$ is decided by maximizing the Lagrangian for a particular subcarrier n, i.e., $\pi^*_{n,k}=1$ if $\pi^*_{n,k} = \underset{\pi_{n,k}}{\arg\max}\ L_n(\pi_{n,k},P_k^{n*},\alpha,\beta,\gamma,\zeta)$ and that user has not been assigned any other subcarrier. If that is not the case, then by iterative procedure a user is identified which has not been assigned to any subcarrier. This ensures that, each user gets only one subcarrier.

Till now, the optimal values of primal variables, i.e., P_k^{n*} and $\pi^*_{n,k}$ are evaluated for a given set of dual variables. Now, the second sub-problem needs to be solved, where Lagrange dual function $g(\alpha,\beta,\gamma,\zeta)$ is minimized over the dual variables in order to evaluate the optimal value of dual L^*_{dual}. The dual problem is always convex in nature irrespective of the structure of primal problem [45]. Therefore, the dual optimal is obtained by subgradient method, where the variables are updated as follows:

$$\begin{aligned}\alpha^{(i+1)} &= \left[\alpha^{(i)}-\delta^{(i)}\Big(P_S-\sum_{k=1}^{K}\sum_{n=1}^{\mathbb{N}}P_k^{n*}\Big)\right]^+,\\ \beta_k^{(i+1)} &= \left[\beta_k^{(i)}-\delta^{(i)}\Big(\sum_{n=1}^{\mathbb{N}}\pi^*_{n,k}r^*_{n,k}-R_o\Big)\right]^+,\forall k\in\mathcal{K},\\ \gamma^{(i+1)} &= \left[\gamma^{(i)}-\delta^{(i)}\Big(R^{bh}_{max}-\sum_{k=1}^{K}\sum_{n=1}^{\mathbb{N}}\pi^*_{n,k}r^*_{n,k}\Big)\right]^+,\\ \zeta_n^{i+1} &= \left[\zeta_n^{(i)}-\delta^{(i)}\Big(I_{th}-\sum_{k=1}^{K}P_k^{n*}\Psi_n\Big)\right]^+,\forall n\in\mathcal{N}\end{aligned} \tag{24}$$

where $[\cdot]^+$ is the rectifier function. This condition is necessary, because the dual variables must be non-negative real numbers in order to satisfy the complementary slackness conditions of the original primal problem. Dual variables have non-zero values only for the active or tight constraints, and they are zero for all the non-active constraints to satisfy the complementary slackness condition. The step size $\delta^{(i)}$ at i^{th} iteration is chosen according to the constant step size policy and independent of iteration number. It is observed that, the algorithm converges to a value proportional to this constant step size within a finite number of iterations [46].

The optimal power allocation is solved for every possible user-subcarrier assignment at each iteration. Also, the dual variables are to be updated. This requires to update a total of $(K+\mathbb{N}+2)$ dual variables in each iteration. Moreover, there are $K\times\mathbb{N}$ power allocations solved at each iteration. If the iteration for subgradient method converges after n_{itr}, the time complexity would be $\mathcal{O}(n_{itr}(K\cdot\mathbb{N}+K+\mathbb{N}+2))$, which is relatively high for the considered subcarrier assignment problem [44]. Therefore, it is important to come up with a more efficient scheme to speed-up the resource allocation problem.

B. Proposed sub-optimal solution

To propose a sub-optimal solution, the analogy of conventional water-filling method is explored, where the sum rate is maximized by allocating more power to the user having better channel condition, and vice-versa [47]. In this method, possible range of allowed power is evaluated for each user based on their respective channel conditions. Then, optimal power allocated to each user is obtained by solving the optimization problem with an objective of total sum rate maximization. The detailed procedure to obtain the sub-optimal solution is described below as follows:

i) To each user assign the subcarrier with best channel conditions and which has not been assigned to any other user.

ii) Using the user-subcarrier assignment in (i), evaluate the minimum and maximum allowed power by satisfying the rate guarantee constraint $(\mathcal{C}2)$ and the tolerable interference constraint $(\mathcal{C}7)$, respectively, of the optimization problem $(\mathcal{P}_2)$. If k^{th} user is assigned to n^{th} subcarrier, then the minimum and maximum allowed power budget for user k is obtained as follows:

$$P_{min,k} = (2^{\frac{R_o}{BW}} - 1)\Big(\frac{N_o + I_{th}}{G_{main} H_k^n}\Big), \quad P_{max,k} = \frac{I_{th}}{G_{side} H_k^n}. \tag{25}$$

iii) Based on the refined range of transmitted power obtained in step (ii), the optimal power allocation problem is formulated as follows:

$$\begin{aligned} (\mathcal{P}_{\mathbf{sub-opt}}): \ & \underset{P_k}{\text{maximize}} \ \sum_{k=1}^{K} r_k, \\ \text{subject to:} \quad & (\mathcal{C}_{s1}) \quad \sum_{k=1}^{K} P_k \le P_S, \\ & (\mathcal{C}_{s2}) \quad P_k \ge P_{min,k}, \quad \forall k \in \mathcal{K}, \\ & (\mathcal{C}_{s3}) \quad P_k \le P_{max,k}, \quad \forall k \in \mathcal{K}. \end{aligned} \tag{26}$$

This maximization problem is a concave optimization problem, because the objective function is a concave function of power allocated to the users, i.e., P_k and all the constraints are linear. Hence, *Karush–Kuhn–Tucker* (KKT) point will be the unique global optimal solution to this problem; and KKT point is obtained by using primal dual interior point method.

iv) The backhaul constraint mentioned in $(\mathcal{C}3)$ is verified by the user-subcarrier association obtained in step (i) and the optimal power allocation in step (iii). If the constraint $(\mathcal{C}3)$ is satisfied then stop the process. Otherwise, starting with the user with least channel gain assign minimum allowed power, till backhaul rate constraint is satisfied.

The computational complexity of the proposed sub-optimal solution is $\mathcal{O}(n_{p-d} + K)$, where n_{p-d} denotes the number of iterations required to find the KKT point. Thus, sub-optimal strategy reduces the computational complexity significantly, and it efficiently solves the resource allocation problem.

1) Optimality gap: The only source of heuristics in the sub-optimal algorithm is due to the user-subcarrier assignment problem. In general this is an integer-programming problem and solving by iterating over every possible combination is restrictive due to huge time complexity. For $\mathbb{N}$ total orthogonal subcarriers, the probability of any particular subcarrier 'n' being optimal for any arbitrary user is $\frac{1}{\mathbb{N}}$. Following on the same analogy, the probability of subcarrier 'n' being optimal for any k users is $\frac{1}{\mathbb{N}^k}$.

C. Comparison benchmark schemes

To compare the performance of the proposed optimal and sub-optimal algorithm, two other schemes, namely, *equal power allocation* and *random channel assignment* are also proposed. These schemes also satisfy all the constraints of the optimization problem $(\mathcal{P}_2)$. However, the choice of solution is based on intuition rather than in an optimal sense.

1) Equal power allocation: As the name suggests, in this method equal power is allocated to each user irrespective of the channel gains. The user-SC assignment to each user is the same as in the sub-optimal scheme. The brief procedure is as follows:

i) User-SC assignment: For each user pick that particular subcarrier which has not been matched to any other user and have the best channel gain for that user.

ii) Calculate $P_{eq} = \frac{P_{max}}{K}$. Also evaluate the maximum $P_{max,k}$ and minimum $P_{min,k}$ allowed power budgets for each user from $(\mathcal{C}2)$ and $(\mathcal{C}7)$ of $(\mathcal{P}2)$ analogous to (25). Finally to allocate power, the below-mentioned rule is followed:

$$\begin{aligned} \textbf{if } (P_{eq} < P_{min,k}) \quad & \Rightarrow P_k^n = P_{min,k}, \\ \textbf{if } (P_{eq} > P_{max,k}) \quad & \Rightarrow P_k^n = P_{max,k}, \\ \textbf{else:} \quad & P_k^n = P_{eq}. \end{aligned}$$

iii) Verify the backhaul constraint $(\mathcal{C}3)$ after the power allocation is done in step (ii). If the constraint is satisfied, then stop the process. Otherwise, starting with the user with least channel gain, assign minimum allowed power till backhaul rate constraint is satisfied.

2) Random channel assignment: In this method, both SC-user assignment and power allocation are done randomly. The brief procedure is as follows:

i) Randomly allocate subcarriers to users ensuring that a single SC is assigned to only one user.

ii) Evaluate the maximum $P_{max,k}$ and minimum $P_{min,k}$ allowed power budgets for each user from $(\mathcal{C}2)$ and $(\mathcal{C}7)$ of $(\mathcal{P}_2)$ analogous to (25). Then generate a random number for power allocation between $P_{min,k}$ and $P_{max,k}$ for each user, and allocate that much power to that subcarrier.

iii) Check the backhaul constraint $(\mathcal{C}3)$ after step (ii). If the constraint is satisfied, then stop the process. Else, starting with the first user, assign minimum allowed power till backhaul rate constraint is satisfied.

V. Numerical Simulation Results

In this section, numerical evaluation of the analysis presented in the previous sections is performed. The users are considered uniformly distributed in a circular area. The total area is divided into 16 sectors. The transmission antenna array for a single sector contains 64 elements to form a directional beam, whereas the receiver antenna is assumed to be omnidirectional. Nakagami fading with shape parameter 3 is considered to incorporate the effect of small-scale fading in the channel between mUBS to a user, path loss and shadowing are considered as described in Section II-B. The value of different parameters considered for simulation are taken from [20], [23]–[25] and are listed in Table III. The numerical simulations are carried out in MATLAB.

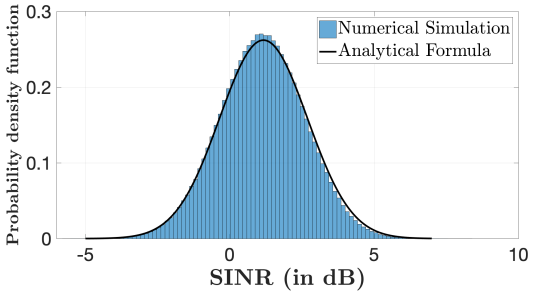

Figure 3: The probability density function of SINR obtained from analysis and simulation.

Table III: Numerical values of different parameters used in simulation.

Parameter	Interpretation	Value
P_S	mUBS total transmit power	10 W
R_o	Minimum rate guarantee	1 bps/Hz
R_{max}^{bh}	Maximum backhaul capacity	200 bps/Hz
N_o	Noise Power density	-174 dBm/Hz
B	Bandwidth	20 MHz
f_{Ghz}	mmWave Carrier frequency	28 GHz
h	Default mUBS height	100 m
I_{th}	Interference threshold	-40.98 dBm
$\lvert\mathcal{S}\rvert$	Total number of sectors	16
$\mathfrak{N}$	Number of antenna array elements	64
$\mathbb{N}$	Number of subcarriers	32
K	Number of users in each sector	16
$\mathcal{R}_a$	Radius of the area served by mUBS	100 m

A. SINR distribution

The probability distribution of SINR obtained from analysis (see (10)) and from numerical simulations are shown in Fig. 3. It can be observed that, the distribution obtained from the analysis closely matches with that obtained from numerical simulation. The distribution shown in Fig. 3 considers simultaneous transmission in all sectors. The SINR is quite low, which is apparently due to high interference.

B. Convergence of the algorithm

The optimal algorithm discussed in Section III involves subgradient method to optimize the dual problem. All primal and dual variables are updated during optimization process in each iteration. The convergence of the optimization problem validates the accuracy of optimal solution. However, it takes large number of iterations to converge towards the optimal solution. The variation of dual variable α associated with the power constraint $(\mathcal{C}1)$ and dual variable γ associated with the backhaul constraint $(\mathcal{C}3)$ of $\mathcal{P}_1$ are shown in Fig. 4(a) and Fig. 4(c), respectively. Both of these dual variables converge at non-zero values, which indicate complementary slackness condition is satisfied. This reveals that the maximum power budget, as well as full capacity of backhaul link are being used, such that both of these constraints are tight.

On the other hand, variation of β_k associated with the minimum rate guarantee to user k and ζ_n corresponding to the interference threshold are shown in Fig. 4(b) and Fig. 4(c), respectively. The dual variables $\{\beta_k\}$ are non-zero for

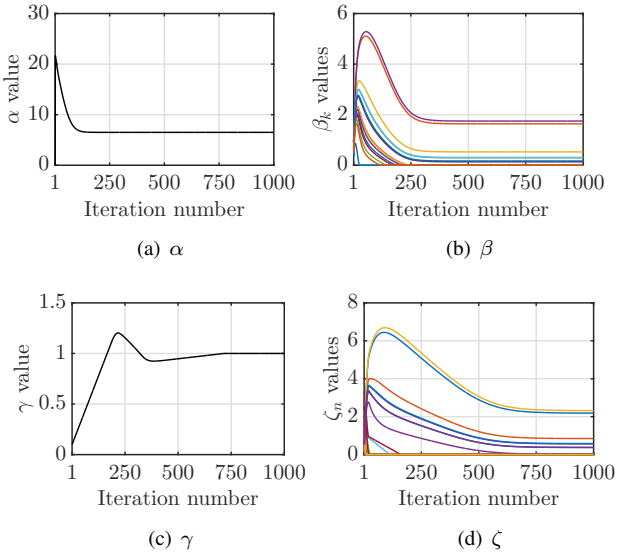

Figure 4: Variation of dual variables over successive iterations.

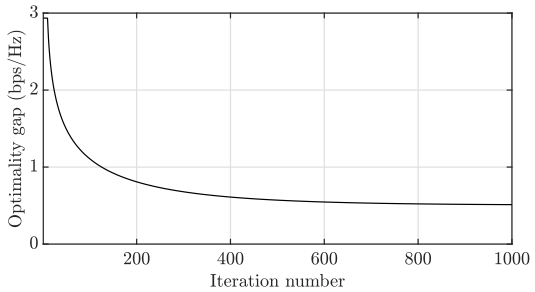

Figure 5: Variation of optimality gap per user over successive iterations.

the users with the rate equal to the minimum threshold requirement. In contrast, β_k is zero for the users whose rate exceed the minimum threshold. These variations corroborate the complementary slackness condition. The dual variable ζ_n also adheres to the same reasoning.

C. Optimality gap

In order to develop a fast and efficient solution to the resource allocation problem in $(\mathcal{P}_2)$, a sub-optimal solution is proposed by solving in the primal domain and heuristically allocating subcarriers to the users. However, it is very important to estimate the gap between optimal and sub-optimal solutions to validate the accuracy of sub-optimal solution. To illustrate this, the variation of optimality gap per user between optimal and sub-optimal algorithm is shown in Fig. 5 against number of iterations of the optimal method. One can observe that the gap decreases as the number of iteration increases and tends to saturate. The gap is 0.51 bps/Hz which is approximately 5%, that is within the tolerable range. Thus, 5% optimality gap for each user is leveraged to speed up the optimal solution estimation process, and hence mUBS resources can be allocated instantly to the users.

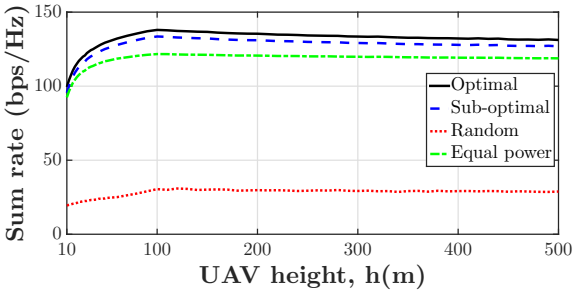

Figure 6: Variation of sum rate against mUBS height, with $P_S = 10$ W, $R_o = 1$ bps/Hz, and $R_{max}^{bh} = 200$ bps/Hz.

D. Optimal height evaluation

The impact of hovering altitude of mUBS on sum rate is shown in Fig. 6. It is observed that the sum rate is low at lower altitudes; it increases with height and then again starts decreasing. This variation in sum rate can be explained by the underlying changes in the path loss as the UAV height changes. Path loss experienced by a user is very high at low altitude due to low LOS probability and high NLOS probability. Also, the path loss exponent value 2.92 for NLOS signal is high compared to the same path loss exponent for LOS which is 2. As the height increases, the total path loss decreases due to the availability of better LOS connectivity. But, if the height continues to increase, the distance based path loss dominates and the sum rate starts to decrease. This result suggests an optimal hovering altitude of mUBS to achieve the maximum sum rate.

Several government agencies, such as Federal Aviation Administration (FAA) [48] and European Union Aviation Safety Agency (EASA) [49], have defined the regulations for safe and reliable operations of UAV. As per these operational limits, hovering altitude of UAV in this work is considered up to 500 m [50]. Several commercial UAVs are available in the market dedicated for different applications, which can operate at such altitudes by carrying sufficient payloads [19].

E. Maximization of sum rate

The variation of achieved sum rate against total allowed transmitted power P_S, is shown in Fig. 7(a). It is noticed that all schemes except random SC assignment saturates to a steady state value. The saturation of sum rate also validates optimality of the solution along with convergence. The amount of power transmitted to each user by mUBS will increase as P_S increases, which increases the interference experienced by the users in different sectors, and it tends to the tolerable limit I_{th}. This restricts further increase in transmit power to each user, and hence the performance does not improve by raising the value of P_S.

Fig. 7(b) shows the variation of sum rate against the minimum rate R_o required by each user. The minimum transmitted power to each user increases with increase in R_o in order to enhance the rate. If R_o continues to increase, then it is also required to increase the transmitted power to each user. This leads to increased interference. After some value of R_o, interference becomes intolerable due to high transmitted power

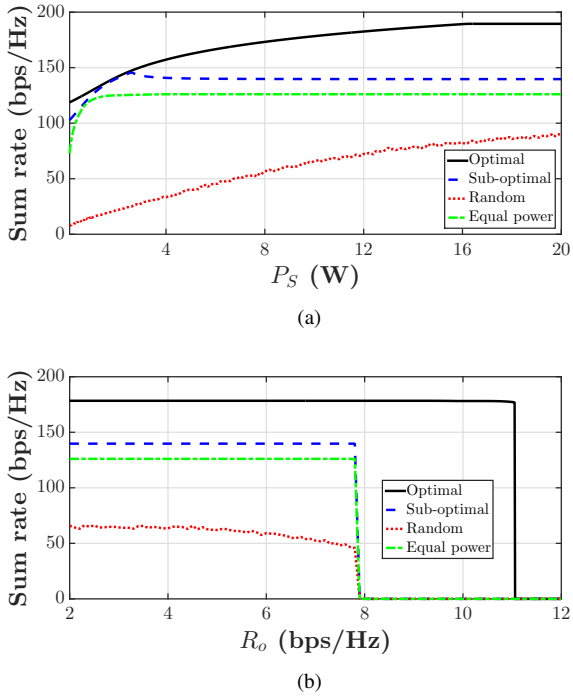

Figure 7: Variation of sum rate against (a) maximum allowed source power P_S, with $R_o = 1$ bps/Hz, $R_{max}^{bh} = 200$ bps/Hz, and (b) minimum rate guarantee given to each user, with $P_S = 10$ W, and $R_{max}^{bh} = 200$ bps/Hz.

to the users and the rate guarantee to some of the users is not ensured. This leads to violation of $(\mathcal{C}2)$ constraint, and therefore a sudden fall in sum rate, which indicates that optimization problem enters into infeasible region.

The effect of capacity of backhaul link R_{max}^{bh} is captured in Fig. 8(a), where R_{max}^{bh} dictates the sum rate. Two regions, namely, backhaul-constrained and backhaul-independent are observed due to this limitation. In backhaul-constrained region, the achievable sum rate is limited by R_{max}^{bh}, for a given value of other variables. On the other hand, the sum rate does not depend on R_{max}^{bh} in backhaul-independent region, and it makes constraint $(\mathcal{C}3)$ insignificant due to very high backhaul capacity. This observation indicates the importance of inclusion of backhaul link in UAV-assisted cellular architecture.

Variation of total sum rate versus the number of users served is shown in Fig. 8(b). It is observed that the sum rate increases monotonically with number of users for all the benchmark schemes. But, the increment is not in a proportionate manner, i.e., it is not linear. The SC assignment overlaps for users in different sectors for crowded scenario, which is responsible for interference. In contrast, the SC assignment can be mutually exclusive for lesser number of users, which avoids interference. Also, SC acquisition is relatively competitive in case of large number of users, which significantly reduces the chance of a user being allocated a SC with good channel conditions. Further, this shows that the proposed transmission scheme can provide minimum rate guarantee to the users equal to number of subcarriers.

Remark 1. *QoS in terms of minimum rate guarantee required*

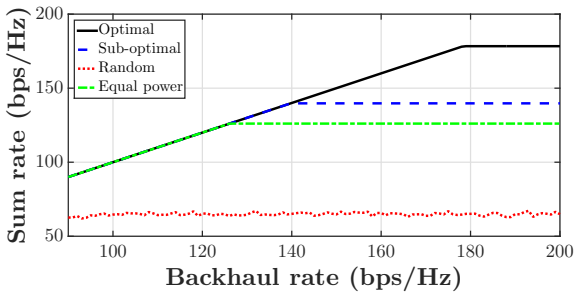

(a)

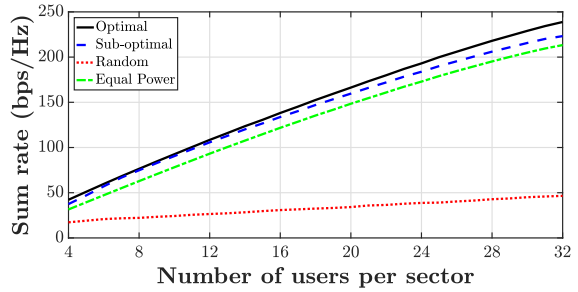

(b)

Figure 8: Variation of sum rate against (a) backhaul capacity, with $P_S = 10$ W, $R_o = 1$ bps/Hz, and (b) number of users per sector, with $P_S = 10$ W, $R_o = 1$ bps/Hz, and $R_{max}^{bh} = 250$ bps/Hz.

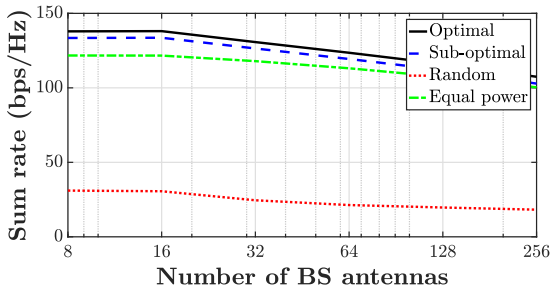

Figure 9: Variation of sum rate against number of antenna elements in mUBS, with $P_S = 10$ W, $R_o = 1$ bps/Hz, and $R_{max}^{bh} = 200$ bps/Hz.

by individual user has a strong impact on overall performance because mUBS cannot satisfy arbitrarily high data rate requirements of each user in the group.

Remark 2. *The mUBS is only able to serve users if the total requested sum rate is less than the wireless backhaul link capacity. Hence, the inclusion of backhaul constraint is an important aspect of system design for UAV-enabled mmWave communication cellular system.*

F. Effect of number of mUBS antennas

The impact of varying the number of antennas on mUBS is shown in Fig. 9. As captured in the analysis in Section II, the gain of antenna array increases as the number of antenna elements is increased and hence the rate of a one-to-one link should increase as well. The sum rate of all users indeed increases to some extent as the number of antennas are doubled

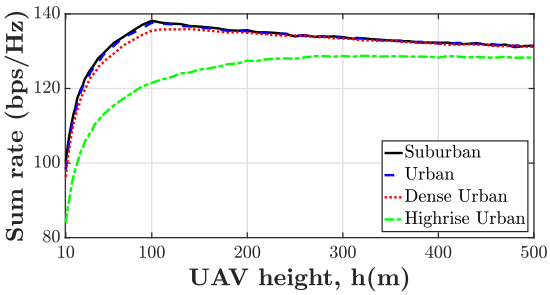

Figure 10: Variation of sum rate against mUBS height for different simulation environments, with $P_S = 10$ W, $R_o = 1$ bps/Hz, and $R_{max}^{bh} = 200$ bps/Hz.

from 8 to 16. However, the sum rate decreases as the number of antenna elements are further increased. The reason for this non-obvious behavior is that the ground projection of antenna array starts to decrease as the number of antenna elements is increased, and after a certain value the beam projection is not able to cover the entire area with sufficient signal strength. Since the users can be located anywhere within the cell of a predefined radius, with narrowed down beam the rate coverage to some of them decreases, and as a result the sum rate decreases.

G. Performance in different environments

In order to observe the effect of different channel environments, the variation of sum rate against mUBS height is shown in Fig. 10 that is achieved based on the optimal resource allocation algorithm. The LOS probability parameters for different environments are taken from [20]. Except for highrise urban, the performance in all other environments are very close, which is because the average heights of building are nearly the same in these environments. The performance in suburban environment is best among these, because the building density is minimum here. This is followed by urban and dense urban scenarios. As the mUBS height increases above a certain value, the sum rate performance in all the environments tends to converge. This is because the pathloss at a larger altitude is dominated by distance based decay instead of availability of LOS link, and path distances are nearly the same in different environments.

H. Comparative study

Till now, the results for the analysis presented in Section II-IV were illustrated, where the side lobe gain of transmitter antenna mounted on mUBS as well as the capacity of backhaul link were taken into consideration while doing resource allocation to the users. In order to demonstrate the impact of these considered features, we have illustrated the following two cases:

- *Case 1:* This corresponds to the scenario where the optimal solution of $\mathcal{P}_2$ is evaluated by considering the gain of side lobes of transmitter antenna and capacity of backhaul link.
- *Case 2:* This corresponds to the scenario where the optimal solution of $\mathcal{P}_2$ is evaluated without considering

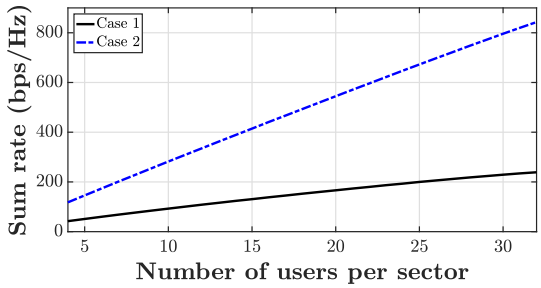

Figure 11: Variation of sum rate against number of users per sector, with $P_S = 10$ W, and $R_o = 1$ bps/Hz. Case 1: optimal solution to problem $\mathcal{P}_2$ with $R_{max}^{bh} = 250$ bps/Hz; Case 2: optimal solution to problem $\mathcal{P}_2$ without backhaul constraint and 0 side lobe gain in the antenna array model.

the gain of side lobe of transmitter antenna, and the capacity of backhaul link is considered unlimited.

The sum rate variation against number of users for these two cases is shown in Fig. 11. It is noticed that the sum rate in *Case 1* is much less compared to that in *Case 2*. In *Case 2*, there is no interference to other sectors, and hence there is no limitation on the transmit power by mUBS, which leads to a higher data rate. Further, the relaxation on backhaul capacity ensures that the data rate of front haul users can be arbitrarily increased. Due to these reasons, the sum rate in *Case 2* is nearly 3 times more than that in *Case 1*. However, *Case 2* is an ideal scenario and far from real-life deployment scenario. Resource allocation according to *Case 2* will lead to overestimating the performance. This comparative study reveals the importance of accounting for the effects of side lobe gain of transmitter antenna and limited capacity of backhaul link on the performance, which is the case in real-life deployment scenario.

Remark 3. *The system design without considering the side lobe gain of transmitter antenna as well as capacity of backhaul link will experience under-resource provisioning, which cannot ensure the QoS of users.*

VI. Conclusion and Future Work

In this paper, optimal resource allocation problem has been investigated for downlink coverage from mmWave transmitter mounted on a UAV. In this approach, a circular user space has been divided into multiple sectors motivated by the highly directional beam generated by antenna array. Side lobe gain of the beams, which cause interference to the other sectors have been taken into consideration in computing probability distribution of signal-to-noise-plus-interference ratio. The formulated optimization problem for resource allocation to maximize the sum rate accounts for the power transmission limit, minimum rate guarantee to each user, and backhaul link capacity. Since the problem is non-convex and involves mixed-integer programming, an asymptotically-optimal solution has been proposed using Lagrangian dual decomposition method. To address high computational overhead, a sub-optimal solution has been presented. Extensive numerical simulations have demonstrated that the proposed algorithm optimally allocates resources to the users, by balancing between interference threshold and minimum rate guarantee. In particular, with optimal power control and subcarrier allocation, it has been demonstrated that mUBS is able to serve users equal to the number of subcarriers with minimum rate requirement of 1 bps/Hz.

Further investigations on the analysis of mUBS in heterogeneous network architecture would be of future research interest. In addition, the multiple UAV deployment scenario needs to be studied. The effects of hovering fluctuations of UAV [51], [52] also needs to be considered in resource allocation and performance deviation from ideal deployment scenario.

References

[1] K. Samdanis and T. Taleb, "The road beyond 5G: A vision and insight of the key technologies," *IEEE Network*, vol. 34, no. 2, pp. 135–141, 2020.

[2] A. E. Saddik, "Multimedia and the tactile internet," *IEEE MultiMedia*, vol. 27, no. 1, pp. 5–7, 2020.

[3] S. K. Sharma, I. Woungang, A. Anpalagan, and S. Chatzinotas, "Toward tactile internet in beyond 5G era: Recent advances, current issues, and future directions," *IEEE Access*, vol. 8, pp. 56 948–56 991, 2020.

[4] A. Ghosh, T. A. Thomas, M. C. Cudak, R. Ratasuk, P. Moorut, F. W. Vook, T. S. Rappaport, G. R. MacCartney, S. Sun, and S. Nie, "Millimeter-wave enhanced local area systems: A high-data-rate approach for future wireless networks," *IEEE J. Sel. Areas Commun.*, vol. 32, no. 6, pp. 1152–1163, June 2014.

[5] T. Nitsche, C. Cordeiro, A. B. Flores, E. W. Knightly, E. Perahia, and J. C. Widmer, "IEEE 802.11ad: directional 60 GHz communication for multi-Gigabit-per-second Wi-Fi," *IEEE Commun. Mag.*, vol. 52, no. 12, pp. 132–141, Dec. 2014.

[6] "Wireless HD specification version 1.1 overview." [Online]. Available: https://www.wirelesshd.org/pdfs/WirelessHD-Specification-Overview-v1.1May2010.pdf

[7] S. Rangan, T. S. Rappaport, and E. Erkip, "Millimeter-Wave cellular wireless networks: Potentials and challenges," *Proc. IEEE*, vol. 102, no. 3, pp. 366–385, Mar. 2014.

[8] T. S. Rappaport, S. Sun, R. Mayzus, H. Zhao, Y. Azar, K. Wang, G. N. Wong, J. K. Schulz, M. Samimi, and F. Gutierrez, "Millimeter wave mobile communications for 5G cellular: It will work!" *IEEE Access*, vol. 1, no. 1, pp. 335–349, Aug. 2013.

[9] M. R. Akdeniz, Y. Liu, M. K. Samimi, S. Sun, S. Rangan, T. S. Rappaport, and E. Erkip, "Millimeter wave channel modeling and cellular capacity evaluation," *IEEE J. Sel. Areas Commun.*, vol. 32, no. 6, pp. 1164–1179, June 2014.

[10] T. Bai and R. W. Heath, "Coverage and rate analysis for millimeter-wave cellular networks," *IEEE Trans. Wireless Commun.*, vol. 14, no. 2, pp. 1100–1114, Feb. 2015.

[11] Minyoung Park and P. Gopalakrishnan, "Analysis on spatial reuse and interference in 60-GHz wireless networks," *IEEE J. Sel. Areas Commun.*, vol. 27, no. 8, pp. 1443–1452, Oct. 2009.

[12] Q. Xue, X. Fang, M. Xiao, and L. Yan, "Multiuser millimeter wave communications with nonorthogonal beams," *IEEE Trans. Veh. Technol.*, vol. 66, no. 7, pp. 5675–5688, July 2017.

[13] O. Semiari, W. Saad, and M. Bennis, "Joint millimeter wave and microwave resources allocation in cellular networks with dual-mode base stations," *IEEE Trans. Wireless Commun.*, vol. 16, no. 7, pp. 4802–4816, July 2017.

[14] S. Hur, T. Kim, D. J. Love, J. V. Krogmeier, T. A. Thomas, and A. Ghosh, "Millimeter wave beamforming for wireless backhaul and access in small cell networks," *IEEE Trans. Commun.*, vol. 61, no. 10, pp. 4391–4403, Oct. 2013.

[15] J. Du, E. Onaran, D. Chizhik, S. Venkatesan, and R. A. Valenzuela, "Gbps user rates using mmwave relayed backhaul with high-gain antennas," *IEEE J. Sel. Areas Commun.*, vol. 35, no. 6, pp. 1363–1372, June 2017.

[16] B. Ma, H. Shah-Mansouri, and V. W. S. Wong, "Multimedia content delivery in millimeter wave home networks," *IEEE Trans. Wireless Commun.*, vol. 15, no. 7, pp. 4826–4838, July 2016.

[17] N. Eshraghi, V. Shah-Mansouri, and B. Maham, "Fair beamwidth selection and resource allocation for indoor millimeter-wave networks," in *Proc. IEEE Int. Conf. Commun. (ICC)*, Paris, France, May 2017, pp. 1–6.

[18] S. Hayat, E. Yanmaz, and R. Muzaffar, "Survey on unmanned aerial vehicle networks for civil applications: A communications viewpoint," *IEEE Commun. Surveys Tuts.*, vol. 18, no. 4, pp. 2624–2661, 4th Quart. 2016.

[19] M. Mozaffari, W. Saad, M. Bennis, Y. Nam, and M. Debbah, "A tutorial on UAVs for wireless networks: Applications, challenges, and open problems," *IEEE Communications Surveys Tutorials*, vol. 21, no. 3, pp. 2334–2360, 2019.

[20] A. Al-Hourani, S. Kandeepan, and S. Lardner, "Optimal LAP altitude for maximum coverage," *IEEE Wireless Commun. Lett.*, vol. 3, no. 6, pp. 569–572, Dec. 2014.

[21] Z. Xiao, P. Xia, and X. Xia, "Enabling UAV cellular with millimeter-wave communication: potentials and approaches," *IEEE Commun. Mag.*, vol. 54, no. 5, pp. 66–73, May 2016.

[22] M. Alzenad, A. El-Keyi, and H. Yanikomeroglu, "3-D placement of an unmanned aerial vehicle base station for maximum coverage of users with different QoS requirements," *IEEE Wireless Communications Letters*, vol. 7, no. 1, pp. 38–41, 2018.

[23] M. Mozaffari, A. Taleb Zadeh Kasgari, W. Saad, M. Bennis, and M. Debbah, "Beyond 5G with UAVs: Foundations of a 3D wireless cellular network," *IEEE Transactions on Wireless Communications*, vol. 18, no. 1, pp. 357–372, 2019.

[24] M. Mozaffari, W. Saad, M. Bennis, and M. Debbah, "Unmanned aerial vehicle with underlaid device-to-device communications: Performance and tradeoffs," *IEEE Trans. Wireless Commun.*, vol. 15, no. 6, pp. 3949–3963, June 2016.

[25] S. Kumar, S. Suman, and S. De, "Backhaul and delay-aware placement of UAV-enabled base station," in *Proc. IEEE INFOCOM wksp.*, Honolulu, HI, USA, Apr. 2018, pp. 1–6.

[26] J. Wang, C. Jiang, Z. Han, Y. Ren, R. G. Maunder, and L. Hanzo, "Taking drones to the next level: Cooperative distributed unmanned-aerial-vehicular networks for small and mini drones," *IEEE Veh. Technol. Mag.*, vol. 12, no. 3, pp. 73–82, 2017.

[27] R. Duan, J. Wang, C. Jiang, H. Yao, Y. Ren, and Y. Qian, "Resource allocation for multi-UAV aided IoT NOMA uplink transmission systems," *IEEE Internet Things J.*, vol. 6, no. 4, pp. 7025–7037, 2019.

[28] Z. Xiao, H. Dong, L. Bai, D. O. Wu, and X. Xia, "Unmanned aerial vehicle base station (UAV-BS) deployment with millimeter-wave beamforming," *IEEE Internet Things J.*, vol. 7, no. 2, pp. 1336–1349, 2020.

[29] N. Rupasinghe, Y. Yapici, I. Guvenc, and Y. Kakishima, "Non-orthogonal multiple access for mmWave drone networks with limited feedback," *IEEE Trans. Commun.*, vol. 67, no. 1, pp. 762–777, Jan. 2019.

[30] J. Chakareski, S. Naqvi, N. Mastronarde, J. Xu, F. Afghah, and A. Razi, "An energy efficient framework for UAV-assisted millimeter wave 5G heterogeneous cellular networks," *IEEE Trans. Green Commun. Netw.*, vol. 3, no. 1, pp. 37–44, Mar. 2019.

[31] M. Gapeyenko, V. Petrov, D. Moltchanov, S. Andreev, N. Himayat, and Y. Koucheryavy, "Flexible and reliable UAV-assisted backhaul operation in 5G mmwave cellular networks," *IEEE J. Sel. Areas Commun.*, vol. 36, no. 11, pp. 2486–2496, Nov. 2018.

[32] W. Yi, Y. Liu, E. Bodanese, A. Nallanathan, and G. K. Karagiannidis, "A unified spatial framework for UAV-aided mmWave networks," *IEEE Trans. Commun.*, vol. 67, no. 12, pp. 8801–8817, 2019.

[33] W. Yi, Y. Liu, Y. Deng, and A. Nallanathan, "Clustered UAV networks with millimeter wave communications: A stochastic geometry view," *IEEE Trans. Commun.*, vol. 68, no. 7, pp. 4342–4357, 2020.

[34] G. Fontanesi, A. Zhu, and H. Ahmadi, "Outage analysis for millimeter-wave fronthaul link of UAV-aided wireless networks," *IEEE Access*, vol. 8, pp. 111 693–111 706, 2020.

[35] X. Wang and M. C. Gursoy, "Coverage analysis for energy-harvesting UAV-assisted mmwave cellular networks," *IEEE J. Sel. Areas Commun.*, vol. 37, no. 12, pp. 2832–2850, 2019.

[36] R. Ma, W. Yang, Y. Zhang, J. Liu, and H. Shi, "Secure mmwave communication using UAV-enabled relay and cooperative jammer," *IEEE Access*, vol. 7, pp. 119 729–119 741, 2019.

[37] C. A. Balanis, *Antenna Theory: Analysis and Design*. John Wiley and Sons, 2012.

[38] W. Khawaja, O. Ozdemir, and I. Guvenc, "UAV air-to-ground channel characterization for mmwave systems," in *Proc. IEEE Vehic. Technol. Conf. (VTCFall)*, Toronto, Canada, Sep. 2017, pp. 1–5.

[39] ——, "Temporal and spatial characteristics of mm wave propagation channels for UAVs," in *Proc. IEEE Global Symposium on Millimeter Waves (GSMM)*, Boulder, Colorado, USA, May 2018, pp. 1–6.

[40] M. Mezzavilla, M. Polese, A. Zanella, A. Dhananjay, S. Rangan, C. Kessler, T. S. Rappaport, and M. Zorzi, "Public safety communications above 6 GHz: Challenges and opportunities," *IEEE Access*, vol. 6, pp. 316–329, 2018.

[41] L. Fenton, "The sum of log-normal probability distributions in scatter transmission systems," *IRE Trans. Commun. Syst.*, vol. 8, no. 1, pp. 57–67, Mar. 1960.

[42] M. Longbrake, "True time-delay beamsteering for radar," in *IEEE NAECON*, Dayton, OH, USA, July 2012, pp. 1–3.

[43] C. Papadimitriou and K. Steiglitz, *Combinatorial Optimization: Algorithm and Complexity*. Prentice Hall, 1982.

[44] W. Yu and R. Lui, "Dual methods for nonconvex spectrum optimization of multicarrier systems," *IEEE Trans. Commun.*, vol. 54, no. 7, pp. 1310–1322, July 2006.

[45] S. Boyd and L. Vandenberghe, *Convex optimization*. Cambridge university press, 2004.

[46] S. Boyd, L. Xiao, and A. Mutapcic, "Subgradient methods." [Online]. Available: https://web.stanford.edu/class/ee392o/subgrad_method.pdf

[47] A. Goldsmith, *Wireless communications*. Cambridge university press, 2005.

[48] "Unmanned Aircraft Systems (UAS) Regulations & Policies," FAA regulation, July 2016. [Online]. Available: https://www.faa.gov

[49] "Flying a Drone," European union regulation, May 2017. [Online]. Available: https://www.easa.europa.eu

[50] J. Wang, C. Jiang, Z. Wei, C. Pan, H. Zhang, and Y. Ren, "Joint UAV hovering altitude and power control for space-air-ground IoT networks," *IEEE Internet Things J.*, vol. 6, no. 2, pp. 1741–1753, 2019.

[51] M. T. Dabiri, H. Safi, S. Parsaeefard, and W. Saad, "Analytical channel models for millimeter wave UAV networks under hovering fluctuations," *IEEE Trans. Wireless Commun.*, vol. 19, no. 4, pp. 2868–2883, 2020.

[52] S. Suman, S. Kumar, and S. De, "Impact of hovering inaccuracy on UAV-aided RFET," *IEEE Commun. Lett.*, vol. 23, no. 12, pp. 2362–2366, 2019.